Inorganic Chemistry
Article
Cite This: Inorg. Chem. XXXX, XXX, XXX−XXX
pubs.acs.org/IC

# Crystal and Magnetic Structures of the Chain Antiferromagnet $CaFe_4Al_8$

Volodymyr Gvozdetskyi,[†,‡] Anatoliy Senyshyn,[§] Roman Gladyshevskii,[‡] and Viktor Hlukhyy*[,†]

[†]Department of Chemistry, Technische Universität München, Lichtenbergstrasse 4, 85747 Garching, Germany
[‡]Department of Inorganic Chemistry, Ivan Franko National University of Lviv, Kyryla i Mefodiya Street 6, 79005 Lviv, Ukraine
[§]Heinz Maier-Leibnitz Zentrum, Technische Universität München, Lichtenbergstrasse 1, 85747 Garching, Germany

*Supporting Information*

**ABSTRACT:** The crystal structure of $CaFe_4Al_8$ was studied by X-ray single crystal and powder diffraction as well as high-resolution neutron powder diffraction. $CaFe_4Al_8$ crystallizes with a tetragonal $CeMn_4Al_8$-type structure, an ordered variant of the $ThMn_{12}$-type (Pearson symbol *tI*26, space group *I*4/*mmm*, $a = 8.777(1)$, $c = 5.077(1)$ Å). Similarly to the well-known A15-type superconductors, the structure of $CaFe_4Al_8$ contains one-dimensional chains of *d*-metal atoms, which are parallel to the crystallographic fourfold axis. $CaFe_4Al_8$ is paramagnetic at room temperature and exhibits long-range antiferromagnetic ordering at about 180 K, combined with a short-range ordered spin arrangement. The magnetic structure, determined by powder neutron diffraction at 4 K, shows that the magnetic moments on the Fe atoms form mirror-inverted chains along the *c*-direction and are slightly canted from the axis.

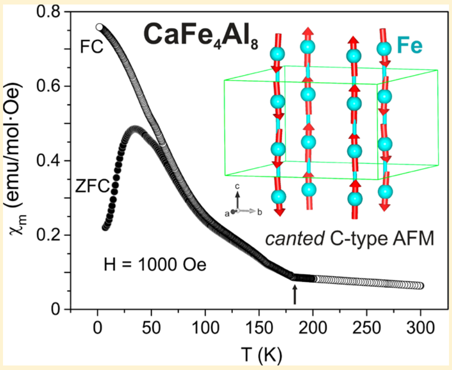

## ■ INTRODUCTION

The discovery of the high-temperature superconductor based on iron $LaFeAsO_{1-x}F_x$ by Hosono et al.[1] has sparked enormous interest in iron-based superconductors with square-planar lattice arrangement of iron atoms.[2] Several families of iron-based superconductors have been identified in recent years, the most prominent being the so-called 1111, 122, 111, and 11 with ZrCuSiAs-, $ThCr_2Si_2$-, CeFeSi-, and anti-PbO-type structures, respectively.[1,3−5] The common structural motif in these families is the $[FeX_{4/4}]$ layer, which contains edge sharing $Fe@X_4$ tetrahedra ($X$ = pnictogen, chalcogen). Besides the square-planar iron layers, also other planar lattice arrangements of transition-metal atoms or one-dimensional chains are interesting regarding the superconductivity. For example, $K_2Cr_3As_3$ with 3d-metal-based quasi-1-D chains was reported to be superconducting.[6] In this compound, similarly to the quasi-two-dimensional superconducting cuprates and iron pnictides, 3d electrons are responsible for unconventional superconductivity. In the well-known and widely used $Nb_3Sn$ (or $Nb_3Ge$) superconductor,[7] which crystallizes in the structure type A15, the Nb atoms form one-dimensional chains in the three orthogonal directions, whereas the Sn (or Ge) atoms form body-centered cubes. The Nb−Nb interatomic distances within the chains are appreciably shorter than the distance between the chains, and these Nb chains respond for the generation of the quasi one-dimensional d-state electronic spectrum of the compound.[8] Recently, the quasi-one-dimensional $BaNbS_3$ compound was reported to be superconducting.[9] In this regard, compounds containing atomic chains of transition metals, especially of iron atoms, may be considered as promising candidates for high-temperature superconductors.

Atomic Fe chains are present e.g. in $RFe_4Al_8$ compounds with extraordinary magnetic properties ($R$ = Sc, Y, Ce, Yb, Lu, Tb, Ho, Er Th, U, Np), which belong to the $CeMn_4Al_8$-type structure (an ordered variant of the $ThMn_{12}$-type).[10,11] Complex magnetic structures with incommensurate spiral components have been observed in, e.g., $RFe_4Al_8$ with $R$ = Tb, Dy, Ho, and Er.[12] The interpretation of the unusual magnetic properties of the $RFe_4Al_8$ compounds is sometimes controversial. For example, at first the $DyFe_4Al_8$ and $HoFe_4Al_8$ compounds were reported to possess magnetic phase transitions attributed to ordering of the iron sublattice into a conical spiral structure at about $T = 25$ K.[13] However, further neutron-scattering experiments showed that the Fe and rare-earth sublattices order magnetically at lower and higher temperatures, respectively, and most of the unusual properties that had been attributed to a spin-glass state[14] are explained by cycloidal ordering of the moments on the magnetic atoms.[15] Soft X-ray resonant scattering experiments indicated that the ordering of the magnetic moments on the $R$ atoms appears to significantly increase the magnitude of the ordered moment on the Fe atoms.[16] The phenomenon of the negative magnetoresistivity, a decrease of the electrical resistivity in the magnetic fields,[17] was recently observed in $RM_4Al_8$ ($R$ = Sc, Y, Ce, Yb, Lu; $M$ = Cr, Mn, Fe).[18] This effect results from the Kondo effect combined with a spin-glass state following crystallo-

**Received:** January 24, 2018

DOI: 10.1021/acs.inorgchem.8b00208
Inorg. Chem. XXXX, XXX, XXX−XXX

graphic disorder (usually due to $M$/Al mixtures). Other intriguing phenomenon of negative magnetization, a decrease of magnetic susceptibility in low magnetic fields[19] observed in several $RT_4Al_8$ phases ($R$ = Sc, Y, Ce, Yb, Lu; $T$ = Cr, Mn, Fe),[20,21] was initially assigned to superconductivity.[22] The bifurcation between the zero-field-cooled (ZFC) and field-cooled (FC) magnetization curves of these phases resembles at first glance the Meissner effect in a superconductor. However, the existence of negative magnetization in these compounds can be explained by a combination of inherent effects such as negative exchange coupling among ferromagnetic (FM), canted antiferromagnetic (AFM), and paramagnetic (PM) sublattices.[19] Small deviations from the stoichiometric 1:4:8 composition (Fe/Al or Fe/$R$ mixture) have a significant effect on the magnetic properties.[23−27] Other $RFe_4Al_8$ compounds with $R$ = Th, U, and Np are antiferromagnetically ordered in G-type spin configurations of the Fe atoms with spin orientations along the $c$-axis.[28]

Taking into account (i) the unusual, often controversial magnetic properties of the $RFe_4Al_8$ compounds, (ii) the fact that $ThMn_{12}$-type derivative intermetallic phases have recently attracted renewed experimental and theoretical interest as possible low-cost hard-magnetic materials,[29] and, last but not least, (iii) the possible superconductivity in quasi-1-D iron compounds, we decided to investigate the crystal and magnetic structure as well as the magnetic properties of the stoichiometric $CaFe_4Al_8$ compound, which contains only one magnetic Fe-sublattice.

## ■ EXPERIMENTAL SECTION

**Synthesis.** Starting materials for the synthesis of $CaFe_4Al_8$ (sample **1**, total mass = 0.4 g) were commercially available elements of high purity: ingots of calcium (AlfaAesar, 99.5%), iron (AlfaAesar 99.98%), and aluminum (ChemPur, 99.99%). At the first stage, the sample with composition Fe:2Al was prepared by melting the elements in an arc furnace equipped with a water-cooled copper hearth (Mini Arc Melting System, MAM-1, Johanna Otto GmbH). To ensure homogenization, the resulting regulus was turned three times. At the next stage, pieces of Ca were stoichiometrically added to the Fe:2Al precursor into a Nb container, which was then sealed. All manipulations were performed in an argon-filled glovebox.

The container was placed into a silica glass tube, which was evacuated and inserted in a vertical resistance furnace (LOBA, HTM Reetz GmbH) connected to a thermo-controller (EUROTHERM). A special heat treatment was performed to obtain single crystals suitable for X-ray diffraction analysis. The silica tube with the sample was heated to 1370 K within 6 h, kept at this temperature for 2 h, cooled to 1070 K at a rate of 0.1 $K\cdot h^{-1}$, kept for 96 h, and finally cooled to room temperature at a rate of 0.1 $K\cdot h^{-1}$. The $CaFe_4Al_8$ compound was found to be stable against air and moisture. Well-shaped single crystals were selected from the sample for further examinations.

**X-ray Investigation.** The purity of the sample **1** was checked using a STOE STADI P powder diffractometer with a Cu $K_{\alpha1}$ source ($\lambda$ = 1.54051 Å, Ge monochromator). To determine the lattice parameters of $CaFe_4Al_8$, Ge powder was used as internal standard. The powder diffractogram (Supporting Information, Figure S1) was corrected using polynomial functions calculated from the matching mode of the experimental and standard Ge-peak positions using the WinXPOW package.[30] Phase analysis was performed using structure models from a database.[10,11] The lattice parameters of $CaFe_4Al_8$ were refined on powder diffraction data using the FullProf Suite program.[31]

Single-crystal intensity data were collected at room temperature using a Stoe IPDS-IIT image-plate diffractometer with graphite-monochromatized Mo $K\alpha$ (0.71073 Å) radiation. Corrections of the raw data for background, polarization, and Lorentz effects were applied. A numerical absorption correction was done using X-Red and X-Shape software.[32,33] Relevant crystallographic data and conditions for the data collections and refinement procedure are listed in Table 1.

**Table 1. Crystal Data and Structure Refinement for $CaFe_4Al_8$ (X-ray Single Crystal Data)**

| empirical formula | $CaFe_4Al_8$ |
|---|---|
| formula weight | 479.32 g/mol |
| space group, $Z$ | $I4/mmm$, 2 |
| unit cell dimensions | $a = b = 8.777(1)$ Å |
| | $c = 5.077(1)$ Å |
| | $V = 391.1(1)$ Å$^3$ |
| calculated density | 4.064 g/cm$^3$ |
| absorption coefficient (Mo $K\alpha$) | 8.72 mm$^{-1}$ |
| $F(000)$ | 456 |
| crystal size | 0.08 × 0.05 × 0.04 mm$^3$ |
| $\theta$ range | 4.6° to 29.0° |
| range in $hkl$ | $\pm12, -12 \le k \le 11, \pm 6$ |
| reflections collected | 3634 |
| independent reflections | 176 ($R_{int}$ = 0.107) |
| reflections with $I \ge 2\sigma(I)$ | 160 ($R_\sigma$ = 0.035) |
| data/parameters | 176/16 |
| GOF on $F^2$ | 1.060 |
| final $R$ indices $[I > 2\sigma(I)]$ | $R1 = 0.025$ |
| | $wR2 = 0.035$ |
| $R$ indices (all data) | $R1 = 0.031$ |
| | $wR2 = 0.036$ |
| largest diff. peak and hole | 0.525 and −0.596 e/Å$^3$ |

The starting atomic parameters for $CaFe_4Al_8$ were obtained by Direct Method with the SHELXS-2014.[34] Subsequently, the structure was refined using SHELXL-2014 (full-matrix least-squares on $F_o^2$)[35] with anisotropic atomic displacement parameters for all atoms. To check the composition, the occupancy parameters were refined in separate least-squares cycles. All the sites were found to be fully occupied. No significant residual peaks were observed in the difference electron-density map.

After the data collection, the single crystal was analyzed by EDX measurements using a Jeol SEM 5900LV scanning electron microscope. No impurity elements heavier than sodium were observed. The analysis revealed the following composition of the crystal (in atomic percentages): Ca = 9(1), Fe = 31(6), and Al = 60(9), which is in good agreement with the composition determined by X-ray and neutron diffraction.

**Neutron Diffraction.** To examine the magnetic structure of $CaFe_4Al_8$, an elastic coherent neutron scattering experiment was performed at the Heinz Maier-Leibnitz Zentrum (Garching bei München, Germany) on the high-resolution diffractometer SPODI.[36] Monochromatic neutrons ($\lambda$ = 1.54832 Å) were obtained at a 155° takeoff using the 551 reflection of a vertically focused composite Ge monochromator. The vertical position-sensitive multidetector (effective height: 300 mm) consisting of 80 $^3He$ tubes and covering an angular spanning of $2\theta = 160°$ was used for the data collection. The measurements were performed in Debye−Scherrer geometry. A 2 g sample (**2**) of $CaFe_4Al_8$ was obtained using the same synthetic route as described above. The powdered sample (volume: ca. 1 cm$^3$) was filled into a thin-wall (0.15 mm) vanadium container (diameter 10 mm) under argon atmosphere and mounted in a top-loading closed-cycle refrigerator. Helium 4.6 (99.996% purity) was used as a heat transmitter. The instantaneous temperature was measured using two thin-film resistance cryogenic temperature sensors Cernox and controlled by a temperature controller LakeShore Cryotronics. Two-dimensional (2D) powder diffraction data were collected at fixed temperatures in the range 4−300 K, where data with higher counting statistics (2.5 h exposure time) were taken at 4 and 300 K. In addition, a number of short exposures (ca. 30 min) was collected at fixed temperatures in the temperature range 10−270 K. The collected 2D diffraction patterns were further corrected for the neutron monitor, geometrical aberrations, and curvature of the Debye−Scherrer rings.[37]

Rietveld refinements were carried out using the software package FullProf (Table 2).[31] The peak profile shape was described by a pseudo-Voigt function. The background of the diffraction pattern was fitted using a linear interpolation between selected data points in nonoverlapping regions. To deduce the evolution of the structural parameters, the Rietveld method was applied. The scale factor, lattice parameter, fractional coordinates of atomic sites, and their isotropic displacement parameters, zero angular shift, profile shape parameters, and half width (Caglioti) parameters were varied during the fitting.

Table 2. Crystal Data and Structure Refinement for $CaFe_4Al_8$ (Pearson Symbol *tI*26, Space Group *I*4/*mmm*, *Z* = 2) at 4 and 300 K (Rietveld Refinement, Neutron Data)

| temperature | 4 K | 300 K |
|---|---|---|
| formula weight | 479.32 g/mol | |
| unit cell dimensions | $a = b = 8.75778(7)$ Å | $a = b = 8.77844(7)$ Å |
| | $c = 5.06328(8)$ Å | $c = 5.07521(7)$ Å |
| | $V = 388.347(8)$ Å$^3$ | $V = 391.101(7)$ Å$^3$ |
| calculated density | 4.099 g/cm$^3$ | 4.070 g/cm$^3$ |
| wavelength ($\lambda$) | 1.54832(5) Å | |
| step scan increment ($2\theta$) | 0.05 | |
| $2\theta$ range | 10−151.9° | |
| program | FullProf | |
| profile points | 3020 | 3020 |
| shape parameter | $\eta = 0.0777$ | $\eta = 0.0950$ |
| Caglioti parameters | $U = 0.04914$ | $U = 0.06174$ |
| | $V = -0.03062$ | $V = -0.03537$ |
| | $W = 0.11538$ | $W = 0.11486$ |
| no. of reflns | 148 | 148 |
| no. of refined parameters | 51 | 57 |
| $R_B$ | 1.20% | 0.47% |
| $R_{magn}$ | 2.47% | |
| $R_P$ | 2.59% | 2.29% |
| $R_{exp}$ | 2.58% | 2.55% |
| $R_{wp}$ | 3.33% | 2.76% |
| $\chi$ | 1.66 | 1.16 |

**Magnetic Measurements.** Magnetic measurements were performed on powdered sample **2** held in a gelatin capsule inside a plastic straw using a Quantum Design MPMS XL-5 SQUID Magnetometer. The data were corrected for the experimentally determined contribution of the sample holder and the diamagnetic contribution of the core electrons (Pascal's constants). Temperature-dependent data were obtained by measuring the magnetic susceptibilities between 1.8 and 300 K in an applied magnetic field (*H*) of 1 kOe. The zero-field-cooled (ZFC) susceptibilities were measured upon heating the sample from 2 to 300 K in a magnetic field of 1 kOe after the sample had been precooled in a zero magnetic field. The field-cooled (FC) susceptibility data were obtained when the sample was cooled from 300 to 2 K in a magnetic field of 1 kOe. Field-dependent measurements were carried out at 2, 10, 25, 150, and 300 K with the field sweeping from −50 to 50 kOe.

**Electronic Structure Calculations.** The electronic structure calculations were performed on the structural model from single crystal data refinement. The linear muffin-tin orbital (LMTO) method in the atomic sphere approximation (ASA) using the tight-binding (TB) program TB-LMTO-ASA was employed.[38] The exchange-correlation term was calculated within the local density approximation (LDA) and was parametrized according to von Barth and Hedin.[39] The radii of the muffin-tin spheres were determined after Jepsen and Andersen.[40] The following valence functions were used for the basis set for the short-ranged atom-centered TB-LMTOs: s valence function for Ca; s, d valence functions for Fe, and s, p valence functions for Al. Ca-4p, −3d, and Al-3d orbitals were treated using a downfolding technique.[41]

The analysis of the chemical bonding was based upon theoretical total, atomic orbital projected density of states (DOS) curves, plots of the crystal orbital Hamilton populations (COHPs),[42] and the "fat bands" representation of the band structure.[43] In the fat band analysis, the character of the atomic orbital is represented as a function of the bandwidth. From the COHP analyses, the contribution of the covalent part of a particular interaction to the total bonding energy of the compound can be obtained. All the COHP curves are presented as the following: positive values are bonding, and negative values are antibonding.

## ■ RESULTS AND DISCUSSION

**Crystal Structure.** $CaFe_4Al_8$ crystallizes in the tetragonal body-centered $CeMn_4Al_8$-type, an ordered variant of the $ThMn_{12}$-type, and is the first ternary compound reported in the Ca/Fe/Al system. The positional parameters and interatomic distances for $CaFe_4Al_8$ are listed in Tables 3 and 4, respectively. Only lattice parameters established from powder X-ray diffraction data and the structure type have previously been reported for $CaFe_4Al_8$: $a = b = 8.85$ Å, $c = 4.89$ Å, $V = 383.0$ Å$^3$.[44] Slightly different lattice parameters were obtained in our experiments (at room temperature): $a = b = 8.77576(8)$, $c = 5.07373(6)$ Å, $V = 390.75(1)$ Å$^3$ (powder X-ray diffraction); $a = b = 8.77844(7)$, $c = 5.07521(7)$ Å, $V = 391.10(1)$ Å$^3$ (powder neutron diffraction); $a = b = 8.7768(13)$, $c = 5.0766(8)$ Å, $V = 391.07(10)$ Å$^3$ (single crystal X-ray diffraction), which are in good agreement with each other. The discrepancy with the earlier published data may be explained by possible Al/Fe substitution. As shown by recent investigations, Al/Fe or *R*/Fe mixed occupancies are often found in $ThMn_{12}$-type related structures and significantly influence the magnetic properties.[23−27] In nonstoichiometric $Sc_{1+x}Fe_{4-x}Al_8$ with nonmagnetic Sc and mixed Fe/Sc occupancy, the iron magnetic moments at 4 K form an incommensurate double cycloid structure.[45] The $ThMn_{12}$-type calcium aluminide $CaCu_4Al_8$ has been reported as a stoichiometric, ordered compound,[46] whereas $CaMn_{4-x}Al_{8+x}$ was reported as ordered ($x = 0$),[47] or with mixed Al/Mn occupancy on the 8*f* site ($x = 1$).[48] Therefore, we determined precisely the crystal and magnetic structures of $CaFe_4Al_8$ based on powder and single crystal X-ray diffraction data and carried out powder neutron diffraction experiments.

Table 3. Atomic Coordinates and Isotropic Equivalent Displacement Parameters for $CaFe_4Al_8$ (X-ray Single Crystal Data, 300 K)

| atom | Wyckoff position | *x*/*a* | *y*/*b* | *z*/*c* | $U_{eq} \times 10^3$ (Å$^2$) |
|---|---|---|---|---|---|
| Ca | 2*a* | 0 | 0 | 0 | 5.2(3) |
| Fe | 8*f* | 1/4 | 1/4 | 1/4 | 4.5(2) |
| Al1 | 8*i* | 0.3402(1) | 0 | 0 | 6.5(3) |
| Al2 | 8*j* | 0.2751(1) | 1/2 | 0 | 4.5(3) |

The following structure description is mainly based on the results of the single crystal data refinement. The main and most important motifs in the structure are one-dimensional chains of iron atoms along the 001 direction (Figures 1a and b). The intrachain Fe−Fe distances of 2.538(1) Å are only slightly elongated as compared to *bcc* iron (2.48 Å)[49] and are significantly shorter than in iron-pnictide superconductors.[10] The Fe chains are separated from each other by a distance of 4.388(1) Å, which excludes direct magnetic exchange interchain

Table 4. Interatomic Distances (Å) for $CaFe_4Al_8$ (X-ray Single Crystal Data, 300 K)

| | | distance (Å) | | | | distance (Å) | |
|---|---|---|---|---|---|---|---|
| Ca | Al1 | 2.9857(13) | (4×) | Fe | Fe | 2.5383(4) | (2×) |
| | Al2 | 3.2156(4) | (8×) | | Al2 | 2.5443(3) | (4×) |
| | Fe | 3.3526(3) | (8×) | | Al1 | 2.6555(11) | (4×) |
| | | | | | Ca | 3.3526(3) | (2×) |
| Al1 | Fe | 2.6555(5) | (4×) | | | | |
| | Al2 | 2.7324(7) | (2×) | Al2 | Fe | 2.5443(3) | (4×) |
| | Al2 | 2.7922(9) | (2×) | | Al1 | 2.7324(7) | (2×) |
| | Al1 | 2.8054(18) | (1×) | | Al2 | 2.7919(12) | (2×) |
| | Ca | 2.783(2) | (1×) | | Al1 | 2.7922(15) | (2×) |
| | Al1 | 2.322(2) | (4×) | | Ca | 3.2156(8) | (2×) |

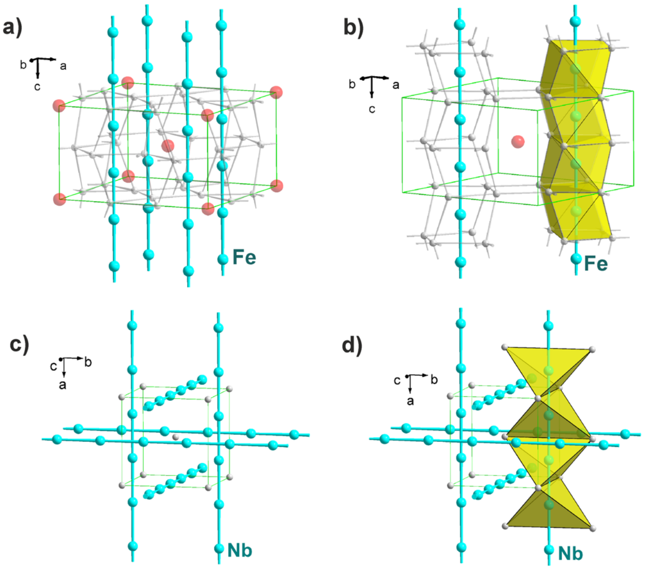

**Figure 1.** Crystal structures of $CaFe_4Al_8$ (a and b) and $Nb_3Sn$ (c and d) compounds underlining the *d*-metal chains. The nearest coordination of *d*-metal atoms by *p*-element is shown (b and d).

interactions. The Fe chains run along the crystallographic $2_1$ axis; therefore, the nearest coordination of Fe atom is a nonregular aluminum eight-vertex polyhedron. Similar well separate one-dimensional *d*-metal chains (*d*(Nb−Nb) = 2.64 Å) are present in the $Nb_3Sn$ superconductor (A15 type), running, in contrast to $CaFe_4Al_8$, in three orthogonal directions (Figures 1c and d).[8] The Nb atoms are tetrahedrally coordinated by Sn atoms in a symmetrical fashion (Nb chains coincide with the 42 axis). Chains of tetrahedrally coordinated Fe atoms (similar to those formed by the Nb atoms in the superconducting A15-type) are found in $AFeCh_2$ chalcogenides ($A$ = Na, K, Rb, Cs, Tl, $Ch$ = S, Se)[50−53] and $Fe_3Se_4(en)_2$[54] with antiferromagnetically ordered moments on the Fe atoms.

The shortest Fe−Al distances (2.544(1)−2.656(1) Å) compare well with the sum of the single bond radii of Fe and Al,[49] as well as with the Fe−Al distances in other intermetallics.[10,11] The Al−Al distances range from 2.732(1) to 2.805(2) Å. The Ca−Al distances lie in the range of 2.988(1)−3.217(1) Å, comparable to the distances in binary Ca/Al compounds,[10,11] whereas the Ca−Fe distance is 3.353(1) Å, which is similar to that found in $CaFe_2Si_2$,[55] $CaFe_2As_2$,[56] or to the Ca−Cu and Ca−Mn distances in $CaCu_4Al_8$ and $CaMn_4Al_8$.[46−48]

The coordination polyhedra of the atoms are presented in Figure S3 (Supporting Information). The coordination around the Ca atom can be viewed as a hexagonal prism with all faces capped: 12 Al atoms and eight Fe atoms (coordination number CN = 20). The iron atoms are coordinated by eight Al atoms, two further Fe atoms, and two Ca atoms in the form of distorted icosahedra (CN = 12). The coordination environment of Al1 is a Frank−Kasper polyhedron (CN = 14) composed of four Fe, nine Al, and one Ca atoms, whereas Al2 is coordinated by four Fe, six Al, and two Ca atoms that form a distorted icosahedron (CN = 12).

**Magnetic Structure.** Analysis of the neutron powder diffraction data obtained at 300 K revealed the major contribution to diffraction pattern coming from $CaFe_4Al_8$ along with traces of FeAl[57] and $Fe_{6.4}Al_{12.6}$.[58] The corresponding powder pattern is shown in Figure S2 (Supporting Information). Due to the low content of $Fe_{6.4}Al_{12.6}$ phase present in the sample of $CaFe_4Al_8$, no standard structure refinement by Rietveld method can be performed; only the Le Bail fitting of this phase was possible.[59] The FeAl phase is present in larger extent, i.e. ca. 1:8 ratio of FeAl to $CaFe_4Al_8$

Table 5. Atomic Coordinates and Equivalent Isotropic Displacement Parameters for $CaFe_4Al_8$ (Neutron Powder Data, $T$ = 4 K) and Magnetic Models Consistent with a k = (0, 0, 0) Propagation Vector

| atom | Wyckoff position | $x/a$ | $y/b$ | $z/c$ | $B_{iso}$, (Å$^2$) |
|---|---|---|---|---|---|
| Ca | 2*a* | 0 | 0 | 0 | 0.82(2) |
| Fe | 8*f* | 1/4 | 1/4 | 1/4 | 0.708(7) |
| Al1 | 8*i* | 0.3425(2) | 0 | 0 | 0.79(2) |
| Al2 | 8*j* | 0.2746(2) | 1/2 | 0 | 1.20(4) |

| irreducible representation | $\Gamma_1$ | $\Gamma_3$ | $\Gamma_5$ | $\Gamma_7$ | $\Gamma_{10A}$ | $\Gamma_{10B}$ |
|---|---|---|---|---|---|---|
| $(x, y, z)$ | $(u,-u,0)$ | $(u,u,v)$ | $(u,-u,0)$ | $(u,u,v)$ | $(u,v,w)$ | $(u,v,w)$ |
| $(-x + 1, -y + 1, z)$ | $(-u,u,0)$ | $(-u,-u,v)$ | $(-u,u,0)$ | $(-u,-u,v)$ | $(u,v,-w)$ | $(u,v,-w)$ |
| $(-x + 1, y, -z + 1)$ | $(-u,-u,0)$ | $(-u,u,-v)$ | $(u,\mathrm{u},0)$ | $(u,-u,v)$ | $(u,-v,w)$ | $(-u,v,-w)$ |
| $(x, -y + 1, -z + 1)$ | $(u,u,0)$ | $(u,-u,-v)$ | $(-u,-u,0)$ | $(-u,u,v)$ | $(u,-v,-w)$ | $(-u,v,w)$ |

DOI: 10.1021/acs.inorgchem.8b00208

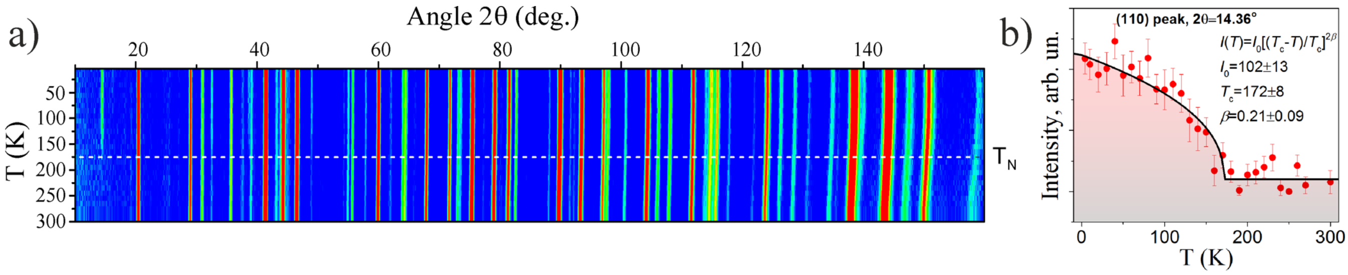

**Figure 2.** Stack of "short-time" neutron diffraction patterns of $CaFe_4Al_8$ collected upon heating (a) and intensity evolution of the (110) superstructure reflection upon heating (b). Log intensities are shown in false colors; the white dashed line highlights the appearance of superstructure reflections.

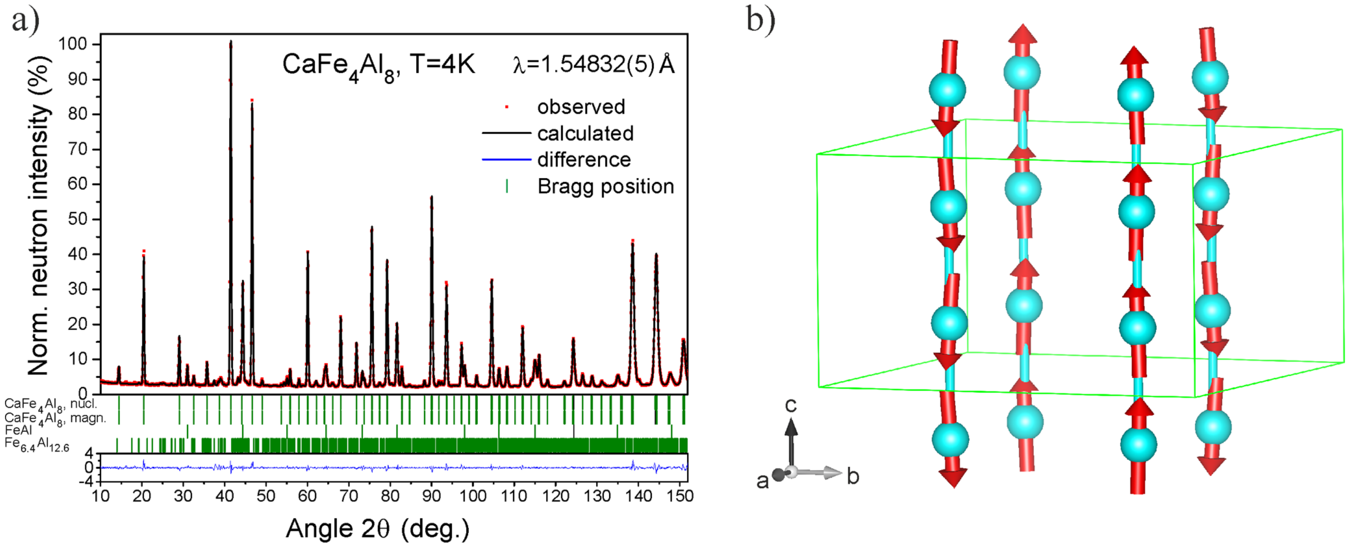

**Figure 3.** Results of Rietveld refinements for neutron powder diffraction of $CaFe_4Al_8$ data at 4 K (a) and orientation of the magnetic moments (b). The calculated positions of the Bragg reflections for the nuclear and magnetic contributions (Γ3-based model) in $CaFe_4Al_8$, FeAl, and $Fe_{6.4}Al_{12.6}$ are shown by the first (top), second, third, and fourth (bottom) rows of vertical tick marks, respectively. Red arrows show the orientation of the magnetic moments; the blue spheres correspond to the iron atoms.

was determined. The structure model of $CaFe_4Al_8$ from the neutron data refinements (Table 5) coincides well with that from the X-ray single crystal data (Table 3), and no Fe/Al mixture was detected.

Sample cooling to 4 K and subsequent data collection resulted in (i) a systematic shift of the major structural peaks to higher $2\theta$ angles and (ii) appearance of superstructure peaks at low $2\theta$ angles. A 2D plot of log diffracted intensities vs the $2\theta$ angle at different temperatures is shown in Figure 2a. The systematic shift of the Bragg reflections upon cooling (especially those at high $2\theta$ angles) toward higher $2\theta$ values may be attributed to a cooling-driven thermal contraction, whereas the appearance of additional intensities at superstructure reflections (110, 130, 310, 112) in the low $2\theta$ range indicates the rise of a long-range magnetic order.

Nonlinear least-squares fits of the thermal peak variation (superstructure 110 reflection, obtained from a "short" data set) with a critical function revealed an ordering temperature $T_c$ of 172(8) K (Figure 2b). No dominating character of the magnetic order can be deduced from the critical exponent, i.e., obtained critical exponent of 0.21(9) was found to be slightly closer to the 2D Ising ($\beta$ = 0.125) than to the 3D Heisenberg ($\beta$ = 0.38) value and might point to a tricritical character of the magnetic transition.

The observed superstructure reflections were found to be consistent with a $\mathbf{k} = (0, 0, 0)$ propagation vector, indicating the identical metrics of the nuclear and magnetic lattices of $CaFe_4Al_8$. Long-range magnetic order of the iron moments is assumed. In a body-centered lattice consistent with $\mathbf{k} = (0, 0, 0)$, the single Fe site with $8f$ Wyckoff symmetry splits into four symmetrically equivalent sites: $(x, y, z)$, $(-x + 1, -y + 1, z)$, $(-x + 1, y, -z + 1)$, $(x, -y + 1, -z + 1)$. Analysis of possible magnetic representations was performed by the Bertaut method[60] and revealed 5 irreducible representations forming a subgroup $\mathbf{G}_\mathbf{k}$ (coinciding with $I4/mmm$ symmetry and leaving the propagation vector **k** invariant). Four irreducible representations (namely Γ1, Γ3, Γ5, and Γ7) are one-dimensional, whereas Γ10 is 2D.

Magnetic structures based on the 1D irreducible representations were constructed and tested by Rietveld refinements (Figure 3a). The obtained parameters characterizing the magnetic order, along with the fit residuals, are listed in Table 5. The structural models built on the irreducible representations Γ1, Γ5, and Γ7 were ruled out during the Rietveld refinements as they were incapable to simulate the majority of the observed magnetic reflections, including the strongest 110 one, thus leaving Γ3 and Γ10. For the 2D case, the number of basic functions needs to be reduced assuming a constant magnetic moment on equivalent iron sites (because they arise from the same orbit). Application of this approach yielded two possible moment arrangements consistent with the irreducible representation Γ10 (marked as $\Gamma_{10A}$ and $\Gamma_{10B}$). Testing of the models based on the irreducible representations $\Gamma_{10A}$ and $\Gamma_{10B}$ resulted in unsatisfactory description of the magnetic intensities.

The best fit was obtained using the magnetic model based on the irreducible representation Γ3 (magnetic space group *I*4′/*mmm*′, group number 139.535, corresponding to an arrangement of mirror-inverted zigzag chains of Fe magnetic moments along the *c*-direction of the tetragonal lattice). This model resulted in a more reliable description of the experimental neutron powder diffraction data and the magnetic R-factor $R_{\mathrm{mag}}$ of 2.47%. A graphical representation of the selected magnetic model is shown in Figure 3b. This arrangement of magnetic moments allows canting of the magnetic moments (*u*, *u*, (*v*), which was, however, found to be less than the corresponding standard deviation (0.037(68), 0.037(68), 0.712(14)) = 0.714(16) $\mu_B$ at 4 K. The resulting magnetic moment is comparable to that reported for $R\mathrm{Fe_4Al_8}$.[61]

No visible magnetoelastic coupling can be seen from the plot of the thermal dependence of the lattice parameters of $\mathrm{CaFe_4Al_8}$, which smoothly and nonlinearly increase upon heating (Figure 4). The *c*/*a* ratio reacts very weakly on temperature changes but displays a nearly constant slope around the ordering temperature (*c*/*a* = 0.578). The first-order Grüneisen approximation was applied to interpret the obtained temperature dependence of $\mathrm{CaFe_4Al_8}$ lattice. In this model, the thermal behavior of the cell volume can be described as follows:

$$V(T) = V_0 + \frac{\gamma}{K_T}U(T) \tag{1}$$

where $V_0$ denotes the hypothetical cell volume at zero temperature, $\gamma$ is the phonon Grüneisen constant, *K* is the bulk modulus, and *U* is the internal energy of the system. Both Grüneisen constant and the bulk modulus are assumed to be temperature-independent, and the Debye approximation for the internal energy *U* in eq 1 takes the form

$$U(T) = U_D(T) = \left[9Nk_BT\left(\frac{T}{\theta_D}\right)^3\int_0^{\theta_D/T}\frac{x^3}{e^x-1}\mathrm{d}x\right] \tag{2}$$

where $\theta_D$ is the Debye temperature, *N* is the number of atoms in the unit cell, and $k_B$ the Boltzmann constant. This approximation provides reasonable descriptions for the cell volumes of different compounds, e.g. FeSi.[62] Besides the cell volumes, the first-order Grüneisen approximation can also be applied to simulate the thermal dependence of the lattice parameters in noncubic systems,[63] where the $\gamma/K$ ratio becomes a fitting constant having no physical measure. Least-squares nonlinear fits of eqs 1 and 2 to the experimental data resulted in an adequate description of the lattice parameters and cell volume of $\mathrm{CaFe_4Al_8}$ (see Figure 4). A Debye temperature $\theta_D$ of 452 ± 11 K was determined. Despite the tetragonal symmetry, the thermal expansion of $\mathrm{CaFe_4Al_8}$ was found to be quasi isotropic.

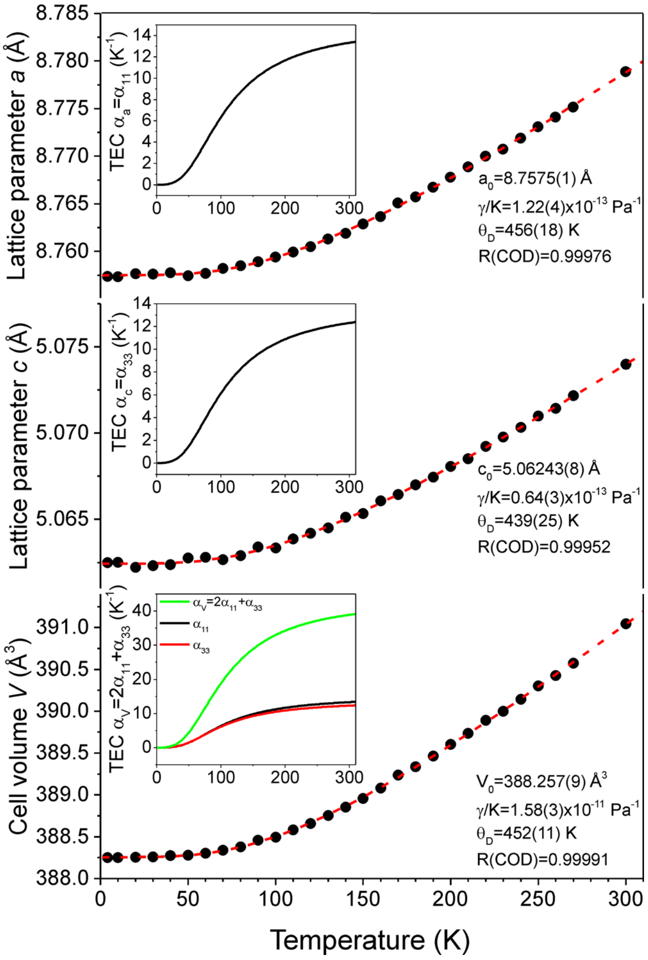

**Figure 4.** Temperature dependence of the lattice parameters and cell volume of $\mathrm{CaFe_4Al_8}$. Lines correspond to the result of data fitting by eqs 1 and 2; calculated thermal expansion coefficients (TEC) $\alpha_l(T)$ = d ln*l*(*T*)/d(*T*) are shown in insets.

**Magnetic Properties.** The absence of sites with mixed Al/Fe occupation in the structure of $\mathrm{CaFe_4Al_8}$ and of any intrinsic magnetic moment on the Ca and Al atoms gave reasons to investigate the magnetic properties of the compound, which depend entirely on the magnetic interactions between the Fe atoms of the Fe chains.

A powdered sample of $\mathrm{CaFe_4Al_8}$ was characterized by susceptibility measurements in ZFC/FC (zero-field-cooled/field-cooled) mode at 20 Oe, 1 kOe, and 5 kOe and by magnetization isotherms at different temperatures (300, 150, 25, 10, and 2 K) with fields up to 50 kOe (Figures 5 and S6). The contribution of the impurity phases to the magnetic susceptibilities of $\mathrm{CaFe_4Al_8}$ is considered as negligible. No magnetic ordering is found in FeAl down to 2 K,[64] whereas $\mathrm{Fe_{6.4}Al_{12.6}}$ (redetermined structure of $\mathrm{FeAl_2}$) undergoes magnetic phase transition at *T* ≈ 32 K and *T* ≈ 12 K accompanied by a spin glass phase formation.[65] Due to low fraction of $\mathrm{Fe_{6.4}Al_{12.6}}$ in the studied sample, no magnetic effects at 32 and 12 K were detected.

The thermal dependencies of the molar magnetic susceptibilities indicate no superconductive transition down to 1.8 K. Below 180 K, the susceptibility increases significantly, indicating the development of magnetic ordering, and a slight bifurcation between the ZFC and FC susceptibilities can be detected, yielding a weak ferromagnetic component to the long-range order (Figure 5a). The ferromagnetic behavior appears more significantly at temperatures of about 1.8–25 K. The value of effective magnetic moment of 3.83 $\mu_B$/Fe atom, obtained by fitting the data with the Curie–Weiss law in the paramagnetic temperature region in the range 190–300 K, is lower than the theoretical values expected for the effective

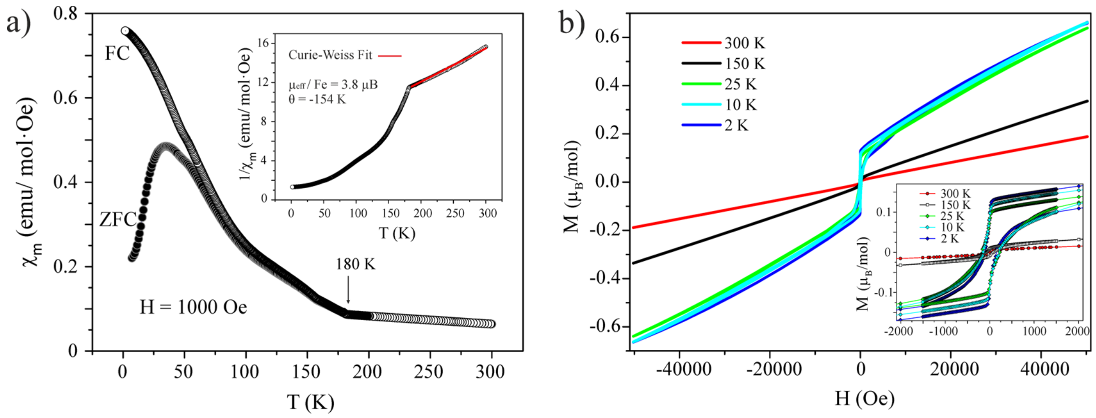

**Figure 5.** Magnetic properties of $CaFe_4Al_8$: molar magnetic susceptibility $\chi_m$ (ZFC/FC mode) and inverse molar magnetic susceptibility $1/\chi_m$ (insert, FC mode) as a function of temperature in a field of 1000 Oe (a); field-dependent magnetization measured at 300, 150, 25, 10, and 2 K (b).

magnetic moments of free $Fe^{3+}$ and $Fe^{2+}$ ions ($\mu_{eff}(Fe^{3+}) = 5.92$ $\mu$B and $\mu_{eff}(Fe^{2+}) = 4.90$ $\mu$B). We believe the reduced moment value to be related by the considerable covalence of Fe—Al bonds and by the direct Fe—Fe interaction within the Fe chain as well (Supporting Information, Figure S4). The Weiss constant determined to be $\theta_p = -154$ K suggests predominant antiferromagnetic interactions (Figure 5a, insert). The irreversibility in the magnetic susceptibilities (ferromagnetic constituent) is also reflected in the magnetization isotherms (Figure 5b). Above the transition temperature $T_c$ (at 300 K), the magnetization is almost linear with no remnant magnetization or coercitivity, whereas below the transition temperature, at 150, 25, 10, and 2 K the remanence increases with decreasing of temperature and at 2 K is about 0.03 $\mu_B$/Fe atom along with a coercitivity of about 120 Oe. The observed ferromagnetic contribution corresponds to the spin canting allowed by the group theory. However, the S-shaped form of the magnetization $M(H)$ isotherms and the cusp-like bifurcation of the ZFC/FC susceptibilities at about 30 K, as well as the low value of the magnetic moment on the Fe atoms estimated from neutron diffraction (0.71 $\mu_B$) compared to the effective magnetic moment from magnetic susceptibility data (3.83 $\mu_B$), indicate the presence of a short-range ordered state along with the long-range ordered canted AFM spin arrangement.

**Electronic Structure Calculations.** To examine the electronic properties of $CaFe_4Al_8$, the total density of states (DOS) as well as the atomic orbital projected density of states (pDOS) were calculated (Figure 6). No band gap at the Fermi level indicates metallic character of the title compound. The DOS of the valence band at lower energies (from −10 to −5 eV) is mainly built up by Al-s states with a small contribution of Al-p states. In the region from −5 to −1 eV, the Fe-d and Al-p partial DOS of similar shape are predominant, indicating hybridization of these orbitals and correspondingly covalent Fe—Al bonds within the $[Fe_4Al_8]$ network. Calculation of the crystal overlap Hamiltonian population (COHP) for this region of the DOS indicates significant Fe—Al interactions, whereas the Al—Al bonding is much weaker (Supporting Information, Figure S4). The electronic bands around the Fermi level, which are often responsible for superconductivity, are dominated mainly by the Fe-3d orbitals. The most remarkable feature in the DOS of $CaFe_4Al_8$ is the appearance of narrow peak at the Fermi level, which provide the dominating contributions to $N(E_F)$. This local maximum, formed predominantly by Fe-d states, can be correlated to a degree of structural or magnetic instability. The situation in the vicinity of the Fermi level in the DOS is mirrored in the fat band analyses (Supporting Information, Figure S5). The analysis of the fat bands reveals that the peak in the DOS at $E_F$ arises from contributions of Fe $3d_{xz,yz}$ orbitals, which correspond to the antiferromagnetic Fe—Fe interactions within the Fe chains. This Fe—Fe bonding is strongest and dominant in the structure of $CaFe_4Al_8$, as shown by the COHP calculations (Supporting Information, Figure S4). The half-filled Fe—Fe antibonding states in the valence region have significant d—d $\sigma^*$ contributions at the Fermi energy $E_F$. The contribution of Al-p and Ca-s,d states to the Fermi surface is small but nonzero.

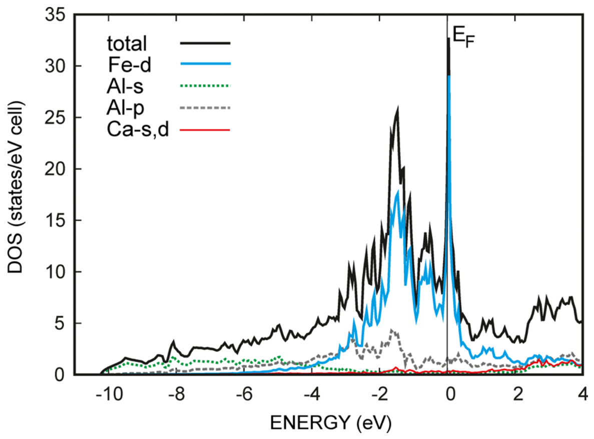

**Figure 6.** DOS and projected DOS calculated for $CaFe_4Al_8$.

## ■ CONCLUSIONS

The crystal structure of $CaFe_4Al_8$ was studied by both X-ray single crystal and high-resolution neutron powder diffraction. The temperature-dependent neutron diffraction study confirms its isostructurality in the temperature range of 4−300 K. Despite the tetragonal symmetry, $CaFe_4Al_8$ is characterized by a quasi-isotropic thermal expansion pointing on its isotropic structural nature. The hypothetical zero Kelvin value for the cell volume, $V_0$, as well as the temperature-independent $\gamma/K$ ratio and the Debye temperature $\theta_D$ were determined as 388.257(9) $Å^3$, $1.58(3) \times 10^{-12}$ $Pa^{-1}$, and 452(11) K, respectively.

Chains of Fe atoms parallel to the fourfold axis are considered to be the most remarkable structural motif of $CaFe_4Al_8$. Similar *d*-metal chains in the $Nb_3Sn$ and other A15 compounds are generally considered as a hint for superconductivity, which motivated us to study the magnetic properties of $CaFe_4Al_8$ in detail. As shown by magnetic measurements and neutron diffraction, this compound exhibits antiferromagnetic ordering at 180 K. The magnetic structure determined at 4 K by neutron diffraction was found to be antiferromagnetic of spin-canted C-type (cC-AFM for short). The magnitude of the ordered magnetic moment on the Fe atoms refined to 0.71(2) $\mu_B$ at 4 K. The magnetic moments form mirror-inverted chains parallel to the *c*-direction of the tetragonal lattice. The antiferromagnetic ordering of the iron sublattice is accompanied by a weak ferromagnetic component resulting from spin canting. The tilt of the magnetic moments, resulting in canted antiferromagnetism, is most probably caused by the unusual nearest coordination of the Fe atoms. As shown by nonspin-polarized electronic structure calculations, in $CaFe_4Al_8$ the antibonding Fe-d orbitals are half-filled at $E_F$, which causes the ordering of magnetic moments at low temperatures. Similarly, the parent compounds of superconducting iron pnictides mostly host a C-type (collinear) antiferromagnetic order within the square-planar Fe layers (with in-plane spin alignment), which produce the pairing interaction for superconductivity. The compounds containing such quasi-one-dimensional transition metal chains are thus quite interesting and promising objects for investigating the correlation between the structural and magnetic peculiarities as well as their relation to superconductivity.

## ■ ASSOCIATED CONTENT

### Ⓢ Supporting Information

The Supporting Information is available free of charge on the ACS Publications website at DOI: 10.1021/acs.inorgchem.8b00208.

Figures of powder patterns, coordination polyhedral, band structure calculations, and magnetic susceptibilities for $CaFe_4Al_8$ (PDF)

### Accession Codes

CCDC 1818947 contains the supplementary crystallographic data for this paper. These data can be obtained free of charge via www.ccdc.cam.ac.uk/data_request/cif, by emailing data_request@ccdc.cam.ac.uk, or by contacting The Cambridge Crystallographic Data Centre, 12 Union Road, Cambridge CB2 1EZ, UK; fax: +44 1223 336033.

## ■ AUTHOR INFORMATION

### Corresponding Author

*E-mail: Viktor.Hlukhyy@lrz.tum.de.

### ORCID

Viktor Hlukhyy: 0000-0002-7533-2670

### Notes

The authors declare no competing financial interest.

## ■ ACKNOWLEDGMENTS

This research was financially supported by the German Research Foundation (Deutsche Forschungsgemeinschaft, DFG, Grant HL 62/3-1) and German Academic Exchange Service (Deutscher Akademischer Austauschdienst, DAAD, Grant A/12/85156).

## ■ REFERENCES

(1) Kamihara, Y.; Watanabe, T.; Hirano, M.; Hosono, H. Iron-Based Layered Superconductor $La[O_{1-x}F_x]FeAs$ (x = 0.05−0.12) with $T_C$ = 26 K. *J. Am. Chem. Soc.* **2008**, *130*, 3296−3297.

(2) Si, Q.; Yu, R.; Abrahams, E. High-temperature superconductivity in iron pnictides and chalcogenides. *Nat. Rev. Mater.* **2016**, *1*, 16017.

(3) Rotter, M.; Tegel, M.; Johrendt, D. Superconductivity at 38 K in the Iron Arsenide $Ba_{1-x}Fe_2As_2$. *Phys. Rev. Lett.* **2008**, *101*, 107006.

(4) Tapp, J. H.; Tang, Z.; Lv, B.; Sasmal, K.; Lorenz, B.; Chu, P. C. W.; Guloy, A. M. LiFeAs: An intrinsic FeAs-based superconductor with Tc = 18 K. *Phys. Rev. B: Condens. Matter Mater. Phys.* **2008**, *78*, No. 060505(R).

(5) Margadonna, S.; Takabayashi, Y.; McDonald, M. T.; Kasperkiewicz, K.; Mizuguchi, Y.; Takano, Y.; Fitch, A. N.; Suard, E.; Prassides, K. Crystal structure of the new $FeSe_{1-x}$ superconductor. *Chem. Commun.* **2008**, 5607−5609.

(6) Bao, J.-K.; Liu, J.-Y.; Ma, C.-W.; Meng, Z.-H.; Tang, Z.-T.; Sun, Y.-L.; Zhai, H.-F.; Jiang, H.; Bai, H.; Feng, C.-M.; Xu, Z.-A.; Cao, G.-H. Superconductivity in Quasi-One-Dimensional $K_2Cr_3As_3$ with Significant Electron Correlations. *Phys. Rev. X* **2015**, *5*, 011013.

(7) Matthias, B. T.; Geballe, T. H.; Geller, S.; Corenzwit, E. Superconductivity of $Nb_3Sn$. *Phys. Rev.* **1954**, *95*, 1435−1435.

(8) Stewart, G. R. Superconductivity in the A15 structure. *Phys. C* **2015**, *514*, 28−35.

(9) Neumeier, J. J.; Smith, M. G. Superconductivity in quasi-one-dimensional $BaNbS_3$. *Phys. C* **2017**, *542*, 1−5.

(10) *Inorganic Crystal Structure Database (on CD-Rom)*, Version 1.9.8; Fachinformationszentrum Karlsruhe: Germany, 2016.

(11) Villars, P.; Cenzual, K. *Pearson's Crystal Data - Crystal Structure Database for Inorganic Compounds (on CD-ROM)*; ASM International: Materials Park, Ohio, 2016/2017.

(12) Schäfer, W.; Grönefeld, M.; Will, G.; Gal, J. Magnetic Helical Ordering in Intermetallic RE-Fe-Al Compounds. *Mater. Sci. Forum* **1988**, *27−28*, 243−248.

(13) Schäfer, W.; Will, G. Neutron diffraction investigation of $DyFe_4Al_8$ and $HoFe_4Al_8$. *J. Less-Common Met.* **1983**, *94*, 205−212.

(14) Talik, E.; Szade, J.; Heimann, J. Spin glass behaviour and magnetic anisotropy in $DyFe_4Al_8$ single crystals. *Phys. B* **1993**, *190*, 361−365.

(15) Paixão, J. A.; Ramos Silva, M.; Sørensen, S. A.; Lebech, B.; Lander, G. H.; Brown, P. J.; Langridge, S.; Talik, E.; Gonçalves, A. P. Neutron-scattering study of the magnetic structure of $DyFe_4Al_8$ and $HoFe_4Al_8$. *Phys. Rev. B: Condens. Matter Mater. Phys.* **2000**, *61*, 6176−6188.

(16) Beale, T. A. W.; Wilkins, S. B.; Hatton, P. D.; Abbamonte, P.; Stanescu, S.; Paixão, J. A. Resonant soft X-ray magnetic scattering from the 4f and 3d electrons in $DyFe_4Al_8$: Magnetic interactions in a cycloidal antiferromagnet. *Phys. Rev. B: Condens. Matter Mater. Phys.* **2007**, *75*, 174432.

(17) Kikugawa, N.; Goswami, P.; Kiswandhi, A.; Choi, E. S.; Graf, D.; Baumbach, R. E.; Brooks, J. S.; Sugii, K.; Iida, Y.; Nishio, M.; Uji, S.; Terashima, T.; Rourke, P. M. C.; Hussey, N. E.; Takatsu, H.; Yonezawa, S.; Maeno, Y.; Balicas, L. Interplanar coupling-dependent magnetoresistivity in high-purity layered metals. *Nat. Commun.* **2016**, *7*, 10903.

(18) Dmitriev, V. M.; Terekhov, A. V.; Suski, W.; Ishchenko, L. A.; Ćwik, J.; Palewski, T.; Kotur, B. Y.; Talik, E. Negative magnetoresistivity of the $RM_4Al_8$ (*R*=Sc, Y, Ce, Yb, Lu; *M*=Cr, Mn, Fe) ternaries with the $ThMn_{12}$-type crystal structure. *J. Alloys Compd.* **2008**, *452*, 217−224.

(19) Kumar, A.; Yusuf, S. M. The phenomenon of negative magnetization and its implications. *Phys. Rep.* **2015**, *556*, 1−34.

(20) Andrzejewski, B.; Kowalczyk, A.; Tolinski, T. Negative magnetisation and absence of superconductivity in $RFe_4Al_8$ (R = Lu, Yb) compounds. *Acta Phys. Pol., A* **2006**, *109*, 561−564.

(21) Andrzejewski, B.; Kowalczyk, A.; Frąckowiak, J. E.; Toliński, T.; Szlaferek, A.; Pal, S.; Simon, C. Unusual negative magnetisation effect in antiferromagnetic $YbFe_4Al_8$ compound. *Phys. Status Solidi B* **2006**, *243*, 295−298.

(22) Drulis, H.; Gaczynski, P.; Iwasieczko, W.; Suski, W.; Kotur, B. Y. Magnetic properties of $YbFe_4Al_8$ intermetallic compound. New antiferromagnetic superconductor. *Solid State Commun.* **2002**, *123*, 391−394.

(23) Gaczynski, P.; Vagizov, F. G.; Suski, W.; Kotur, B.; Iwasieczko, W.; Drulis, H. Magnetic and hyperfine interaction in $RFe_4Al_8$ ($R$ = Ce, Sc) compounds. *J. Magn. Magn. Mater.* **2001**, *225*, 351−358.

(24) Recko, K.; Dobrzynski, L.; Szymanski, K.; Satula, D.; Perzynska, K.; Biernacka, M.; Waliszewski, J.; Zaleski, P.; Suski, W.; Wochowski, K.; Hofmann, M.; Hohlwein, D. Magnetic properties of $ThFe_xAl_{12-x}$ alloys. *Phys. Status Solidi A* **2003**, *196*, 344−347.

(25) Kuznietz, M.; Goncalves, A. P.; Waerenborgh, J. C.; Almeida, M.; Cardoso, C.; Cruz, M. M.; Godinho, M. Magnetic phase diagram of the semiordered alloys $UFe_xAl_{12-x}$. *Phys. Rev. B: Condens. Matter Mater. Phys.* **1999**, *60*, 9494−9500.

(26) Waerenborgh, J. C.; Salamakha, P.; Sologub, O.; Goncalves, A. P.; Serio, S.; Godinho, M.; Almeida, M. $^{57}$Fe Mössbauer spectroscopy study of the $AFe_xAl_{12-x}$ intermetallics ($A$ = Y, Tm, Lu and U, $4 \leq x \leq 4.3$),. *J. Alloys Compd.* **2001**, *317*, 44−51.

(27) Gorbunov, D. I.; Andreev, A. V.; Danis, S.; Pospisil, J. Evolution of magnetism in $LuFe_xAl_{12-x}$ ($4 \leq x \leq 6$) single crystals. *J. Alloys Compd.* **2013**, *563*, 63−71.

(28) Schäfer, W.; Will, G.; Gal, J.; Suski, W. Neutron diffraction studies of the structural and magnetic properties of $AnFe_4Al_8$ ($An$ = Th, U, Np) intermetallic compounds. *J. Less-Common Met.* **1989**, *149*, 237−241.

(29) Körner, W.; Krugel, G.; Elsässer, C. Theoretical screening of intermetallic $ThMn_{12}$-type phases for new hard-magnetic compounds with low rare earth content. *Sci. Rep.* **2016**, *6*, 24686.

(30) *STOE WinXPOW*, Version 3.0.2.1; STOE & Cie GmbH: Darmstadt, 2011.

(31) Rodriguez-Carvajal, J. *FullProf.2k*, Version 5.3; Laboratoire Leon Brillouin (CEA-CNRS): France, 2012.

(32) *X-RED32*, Version 1.48; STOE & Cie GmbH: Darmstadt, Germany, 2008.

(33) *X-SHAPE*, Version 2.11; STOE & Cie GmbH: Darmstadt, Germany, 2008.

(34) Sheldrick, G. M. *SHELXS-2014, Program for the Determination of Crystal Structure*; University of Goettingen: Goettingen, Germany, 2014.

(35) Sheldrick, G. M. *SHELXL-2014, Program for Crystal Structure Refinement*; University of Goettingen: Goettingen, Germany, 2014.

(36) Hoelzel, M.; Senyshyn, A.; Dolotko, O. SPODI: High resolution powder diffractometer. *Journal of Large-Scale Research Facilities JLSRF* **2015**, *1*, A5.

(37) Hoelzel, M.; Senyshyn, A.; Juenke, N.; Boysen, H.; Schmahl, W.; Fuess, H. High-resolution neutron powder diffractometer SPODI at research reactor FRM II. *Nucl. Instrum. Methods Phys. Res., Sect. A* **2012**, *667*, 32−37.

(38) Schilfgaarde, M. v.; Jepsen, O.; Andersen, O. K.; Burkhardt, A.; Paxton, T. A.; Krier, G. *Stuttgart Tight-Binding LMTO-ASA program*, Version 4.7; Max-Planck-Institut für Festkörperforschung: Stuttgart, Germany, 1997.

(39) Barth, U. V.; Hedin, L. A local exchange-correlation potential for the spin polarized case. *J. Phys. C: Solid State Phys.* **1972**, *5*, 1629−1642.

(40) Jepsen, O.; Andersen, O. K. Calculated Electronic-Structure of the Sandwich D(1) Metals $LaI_2$ and $CeI_2$ - Application of New LMTO Techniques. *Z. Phys. B: Condens. Matter* **1995**, *97*, 35−47.

(41) Lambrecht, W. R. L.; Andersen, O. K. Minimal basis sets in the linear muffin-tin orbital method: Application to the diamond-structure crystals C, Si, and Ge. *Phys. Rev. B: Condens. Matter Mater. Phys.* **1986**, *34*, 2439−2449.

(42) Dronskowski, R.; Blochl, P. E. Crystal Orbital Hamilton Populations (COHP) - Energy-Resolved Visualization of Chemical Bonding in Solids Based on Density-Functional Calculations. *J. Phys. Chem.* **1993**, *97*, 8617−8624.

(43) Savin, A.; Nesper, R.; Wengert, S.; Fassler, T. F. ELF: The electron localization function. *Angew. Chem., Int. Ed. Engl.* **1997**, *36*, 1808−1832.

(44) Zarechnyuk, O. S.; Vivchar, O. I.; Ryabov, V. R. X-ray investigation of the systems scandium-iron-aluminium and calcium-iron-aluminium. *Dopov. Akad. Nauk. Ukr. RSR* **1970**, 943−945.

(45) Rećko, K.; Dobrzyński, L.; Senyshyn, A.; Fuess, H.; Szymański, K.; Yu Kotur, B.; Suski, W. Structural and magnetic properties of Sc1.1Fe3.9Al8 alloy. *J. Magn. Magn. Mater.* **2011**, *323*, 1860−1867.

(46) Cordier, G.; Czech, E.; Ochmann, H.; Schäfer, H. Neue Übergangsmetallaluminide des Calciums. *J. Less-Common Met.* **1984**, *99*, 173−185.

(47) Czech, E.; Cordier, G.; Schaefer, H. $CaMn_xAl_{2-x}$ und $CaMn_4Al_8$, ternaere Verbindungen der $MgNi_2$-beziehungsweise $ThMn_{12}$-Struktur. *J. Less-Common Met.* **1983**, *90*, 109−119.

(48) Manyako, N. B.; Yanson, T. I.; Zarechnyuk, O. S. Isothermal sections at 770 K through ternary phase diagrams of the systems Eu (Ca, Sr, Ba) - Mn - Al. *Russ. Metall.* **1988**, *1988*, 212−215.

(49) Emsley, J. *The Elements*; Oxford University Press: Oxford, 1999.

(50) Seidov, Z.; von Nidda, H. A. K.; Tsurkan, V.; Filippova, I. G.; Gunther, A.; Gavrilova, T. P.; Vagizov, F. G.; Kiiamov, A. G.; Tagirov, L. R.; Loidl, A. Magnetic properties of the covalent chain antiferromagnet $RbFeSe_2$. *Phys. Rev. B: Condens. Matter Mater. Phys.* **2016**, *94*, 134414.

(51) Bronger, W.; Kyas, A.; Muller, P. The antiferromagnetic structures of $KFeS_2$, $RbFeS_2$, $KFeSe_2$, and $RbFeSe_2$ and the correlation between magnetic moments and crystal field calculations. *J. Solid State Chem.* **1987**, *70*, 262−270.

(52) Seidov, Z.; Krug von Nidda, H.-A.; Tsurkan, V.; Filippova, I.; Günther, A.; Najafov, A.; Aliyev, M. N.; Vagizov, F. G.; Kiiamov, A. G.; Tagirov, L. R.; Gavrilova, T.; Loidl, A. Magnetic properties of chain antiferromagnets $RbFeSe_2$, $TlFeSe_2$, and $TlFeS_2$. *Bull. Russ. Acad. Sci.: Phys.* **2017**, *81*, 885−887.

(53) Stüble, P.; Röhr, C. Cs[$FeSe_2$], $Cs_3[FeSe_2]_2$, and $Cs_7[Fe_4Se_8]$: Missing Links of Known Chalcogenido Ferrate Series. *Z. Anorg. Allg. Chem.* **2017**, *643*, 1462−1473.

(54) Pak, C.; Kamali, S.; Pham, J.; Lee, K.; Greenfield, J. T.; Kovnir, K. Chemical Excision of Tetrahedral $FeSe_2$ Chains from the Superconductor FeSe: Synthesis, Crystal Structure, and Magnetism of $Fe_3Se_4(en)_2$. *J. Am. Chem. Soc.* **2013**, *135*, 19111−19114.

(55) Hlukhyy, V.; Hoffmann, A. V.; Fässler, T. F. Synthesis, structure and chemical bonding of $CaFe_{2-x}Rh_xSi_2$ ($x$ = 0, 1.32, and 2) and $SrCo_2Si_2$. *J. Solid State Chem.* **2013**, *203*, 232−239.

(56) Ronning, F.; Klimczuk, T.; Bauer, E. D.; Volz, H.; Thompson, J. D. Synthesis and properties of $CaFe_2As_2$ single crystals. *J. Phys.: Condens. Matter* **2008**, *20*, 322201.

(57) Bradley, A. J.; Jay, A. H. The lattice spacings of iron-aluminium alloys. *J. Iron Steel Inst.* **1932**, 339−357.

(58) Chumak, I.; Richter, K. W.; Ehrenberg, H. Redetermination of iron dialuminide, $FeAl_2$. *Acta Crystallogr., Sect. C: Cryst. Struct. Commun.* **2010**, *66*, 87−88.

(59) LeBail, A.; Duroy, H.; Fourquet, J. L. Ab Initio Structure Determination of $LiSbWO_6$ by X-ray Powder Diffraction. *Mater. Res. Bull.* **1988**, *23*, 447−452.

(60) Bertaut, E. F. Representation analysis of magnetic structures. *Acta Crystallogr., Sect. A: Cryst. Phys., Diffr., Theor. Gen. Crystallogr.* **1968**, *A24*, 217−231.

(61) Buschow, K. H. J.; Van der Kraan, A. M. Magnetic ordering in ternary rare earth iron aluminum compounds ($RFe_4Al_8$). *J. Phys. F: Met. Phys.* **1978**, *8*, 921−932.

(62) Vočadlo, L.; Knight, K. S.; Price, G. D.; Wood, I. G. Thermal expansion and crystal structure of FeSi between 4 and 1173 K determined by time-of-flight neutron powder diffraction. *Phys. Chem. Miner.* **2002**, *29*, 132−139.

(63) Senyshyn, A.; Boysen, H.; Niewa, R.; Banys, J.; Kinka, M.; Burak, Y.; Adamiv, V.; Izumi, F.; Chumak, I.; Fuess, H. High-temperature properties of lithium tetraborate $Li_2B_4O_7$. *J. Phys. D: Appl. Phys.* **2012**, *45*, 175305.

(64) Galler, A.; Taranto, C.; Wallerberger, M.; Kaltak, M.; Kresse, G.; Sangiovanni, G.; Toschi, A.; Held, K. Screened moments and absence of ferromagnetism in FeAl. *Phys. Rev. B: Condens. Matter Mater. Phys.* **2015**, *92*, 205132.

(65) Jagličić, Z.; Vrtnik, S.; Feuerbacher, M.; Dolinšek, J. Magnetic properties of $FeAl_2$ and $Fe_2Al_5$. *Phys. Rev. B: Condens. Matter Mater. Phys.* **2011**, *83*, 224427.

DOI: 10.1021/acs.inorgchem.8b00208
*Inorg. Chem.* XXXX, XXX, XXX−XXX